Original article

Phytochemical from Zingiberaceae as a sustainable optical probe for heavy metal determination

Nuttapon Apiratikul [a,b], Pan Tongraung [a], Kulvadee Dolsophon [a,b], Pornthip Boonsri [a], Kriangsak Songsrirote [a,c,*]

[a] Department of Chemistry, Faculty of Science, Srinakharinwirot University, Bangkok 10110, Thailand
[b] Department of Chemistry and Center of Excellence for Innovation in Chemistry, Faculty of Science, Srinakharinwirot University, Bangkok 10110, Thailand
[c] Center of Excellence in Agricultural Innovation and Food Safety, Department of Chemistry, Faculty of Science, Srinakharinwirot University, Bangkok 10110, Thailand

ARTICLE INFO

ABSTRACT

Pinostrobin (PS) extracted from fingerroot was successfully applied as a dual signalling optical sensor that selectively detected Fe^{3+} and Al^{3+} via colorimetric and fluorometric methods, respectively. The selectivity of detection was pH-dependent and was optimal at pH 7. Chelation between PS and Fe^{3+} resulted in the formation of a brown complex with a maximum absorbance of 335.0 nm, while the formation of a colorless complex with Al^{3+} caused an enhancement of fluorescent intensity of PS at the wavelength of 500.0 nm. The linearity range for Fe^{3+} were 1–150 ppm and 0.05–100 ppm for Al^{3+}. The limits of detection were 0.27 ppm for Fe^{3+} and 0.02 ppm for Al^{3+}. Binding stoichiometry for both metal ions to ligand was the same at 1:2 as Fe^{3+}-$(PS)_2$ and Al^{3+}-$(PS)_2$. The brown color of Fe^{3+}-$(PS)_2$ complex can be explained using the crystal field and charge transfer theory. For the Al^{3+}-$(PS)_2$ complex, the fluorescent intensity was considerably enhanced compared to that of free PS because the proton transfer process was inhibited by the complex formation. Theoretical calculation was performed to confirm the complex formation between PS and the metal ions. Based on the proposed complex structure, the binding energies of Fe^{3+} and Al^{3+} complexes were calculated, and the values were found to be −11.45 eV and −19.37 eV, respectively, indicating high stability of the structure and geometry of the metal complexes.

1. Introduction

Contamination of heavy metals in environmental resources has been a global concern for public health because they are highly toxic even at trace levels (Ihedioha et al., 2017; Jaishankar et al., 2014). In addition, heavy metals are non-biodegradable, consequently accumulating in the environment including in water, soil, and living organism (Ali et al., 2019; Wang et al., 2016). Heavy metals are present naturally in the environment and are also discarded through anthropogenic activities (Edelstein et al., 2018; Ihedioha et al., 2017). They generally exist in a form of ion species capable of interacting with other substances and are easily transferred among environmental spheres (Ali et al., 2018; Odika et al., 2020).

Several conventional techniques are used to monitor and determine the level of heavy metal contamination such as inductively coupled plasma optical emission spectrometry (Massadeh et al., 2020), atomic fluorescence spectrometry (Liang et al., 2004), and atomic absorption spectrometry (Assubaie 2015; Tüzen 2003). These analytical techniques offer high accuracy, selectivity, and sensitivity. However, they are hindered by high analysis cost, user skills, and a large sample volume. Therefore, simple and economical approaches for heavy metal determination have been developed including optical sensors, chromogenic and fluorogenic probes using nanoparticles (NPs) (He et al., 2020; Siangproh et al., 2016), quantum dots (QDs) (Liu et al., 2019; Thepmanee et al., 2020), and chemosensors (Zhang et al., 2017). Ironically, these optical sensors produce more heavy metals to the environment and consume a large amount of chemicals in the process of fabrication. Developing an environmentally friendly sensor that is also safe, simple and does not require extensive laboratory skills and a large sample volume has therefore been challenging.

* Corresponding author.
    E-mail address: kriangsaks@g.swu.ac.th (K. Songsrirote).

Metal ions show high potential to form complexes with oxygen, nitrogen, and sulfur containing biological molecules (Adusei-Gyamfi et al., 2019; Petukh et al., 2014). Various herbs have potential to be used in the elimination of heavy metals and detoxification such as turmeric, cumin, onions, garlic, and tea (Qayoom et al., 2017; Winiarska-Mieczan 2018). The interaction between metal ions and natural compounds has been extensively scrutinized (Jing et al., 2017; Shi et al., 2015), and studies have found that phytochemicals such as oligosaccharides, phytochelatins, and polyphenol show promising chelating ability with metal ions (Shi et al., 2015; Kasprzak et al., 2015). In addition, various chemicals from plants have distinguished optical properties in the presence of hydrogen or metal ions (Li et al., 2014; Sigurdson et al., 2016). Consequently, natural products from plants are great candidates for metal ion detection as they are also abundant, sustainable, and safe.

Flavonoids are a group of polyphenolic compounds with a wide variety in chemical structures, characteristics, and biological and chemical activities (Dias et al., 2021). They are the largest group of plant chemicals and over 4,000 different flavonoids have been identified (Kumar et al., 2013). Owing to the carbonyl and hydroxyl groups in the structures, flavonoids generally are able to form complexes with metal ions via coordinate covalent bond (Jomová et al., 2019; Kasprzak et al., 2015). Although a large number of complex formation between flavonoids and metal ions has been investigated, most of these studies focused on biological activities of the complexes on medical applications such as antioxidant, anticancer activities, and neurodegenerative diseases (Kejík et al., 2021; Khater et al., 2019; Rodríguez-Arce et al., 2021). Only a few of these compounds were reported as optical probes for metal ion, such as anthrocyanins, naturally occurring pigments that produce red–purple-blue hues in nature (Sigurdson et al., 2016; Sigurdson et al., 2017). Pinostrobin (PS) is one of major bioflavonoids found in various plants including Zingiberaceae or the ginger family, widely distributed throughout tropical areas (Kanchanapiboon et al., 2020; Rosdianto et al., 2020). As PS can be abundantly extracted, this work aimed to use PS as an optical sensor for heavy metal determination in real water samples. Although the free-form PS is non-florescent and colorless, the PS-metal complexes showed interesting optical behaviors, which could be potentially developed as a sensitive and selective optical sensor for heavy metal detection. Moreover, the mechanism of the complex formation between PS extracted from *Boesenbergia rotunda* (L.) Mansf. (fingerroot) and metal ions was elucidated.

2. Materials and methods

2.1. Chemicals and materials

Metal ion salts were purchased from Sigma-Aldrich. Organic solvents, hydrochloric acid and sodium hydroxide were purchased from commercial suppliers and used without further purification. *Boesenbergia rotunda* (L.) Mansf. (fingerroot) was obtained from Tai-an-jan herbal store, Bangkok in 2021.

2.2. Pinostrobin extraction from fingerroot

Dried rhizomes of fingerroot (3.2 kg) were mashed and extracted exhaustively 5 times with 4 L of *n*-hexane at room temperature. The hexane extract was evaporated to dryness using a rotary evaporator to yield a crude extract. The crude hexane extract was fractionated by quick column chromatography eluting with a gradient of hexane-dichloromethane (50:50 to 0:100). The eluent was collected at every 600 mL producing 5 main fractions. The second fraction was added with cold ethanol to obtain a crude

solid. Recrystallization of the crude solid with hexane-ethanol was performed to obtain pure PS.

2.3. Characterization of extracted pinostrobin

Absorption spectra of PS dissolved in 50 % ethanol were acquired using a spectrophotometer (Agilent 8453 UV–visible spectrophotometer with micro-volume cuvette) and the excitation and fluorescence emission spectra were measured using a fluorometer (Shimadzu RF-5301PC spectrofluoro photometer). Chemical compositions of PS were analyzed using fourier transform infrared (FTIR) spectroscopy in an attenuated reflection mode. FTIR spectra were obtained in the range of wavenumbers from 400 cm^{-1} to 4000 cm^{-1} and 64 scans with a 2 cm^{-1} resolution (Spectrum GX FTIR System, Perkin-Elmer, USA). Proton and carbon nuclear magnetic resonance (^{1}H- and ^{13}C NMR, Bruker Ascend 500), and mass spectrometry (Bruker micrOTOF-II) were also performed to confirm the structure and purity of PS.

2.4. Selectivity of and optimal conditions for metal ion binding

Selectivity of PS on metal ions was determined by monitoring the change in UV–Vis and fluorescent spectra of PS solution with and without the addition of various metal ions at the ratio of 1:1 by volume. The metal ions that caused the change in optical properties were further studied to achieve optimum conditions including pH, concentration of PS, and reaction time for metal ion detection. The pH ranging from 3 to 9 of PS and metal ion solutions were adjusted using 1.0 mM of HCl and 1.0 mM of NaOH.

2.5. Method validation

Figures of merit of the developed method were evaluated. The linear range, limit of detection (LOD), limit of quantification (LOQ), precision, and accuracy of the method were determined. Method validation was performed by measuring the recovery of the standard metal ions spiked in filtered water samples. All analyses were performed in triplicate and compared to those obtained by the conventional inductively coupled plasma (ICP) spectrometry (Perkin Elmer Avio 200). Significant differences between the two groups were identified using a paired sample *t*-test.

2.6. Study of complex formation between pinostrobin and metal ions

Solutions of PS and standard metal ions of the same concentration at pH 7 were mixed at different ratios. Then, the fluorescence intensities of the mixtures were measured at 538.0 nm by fluorophotometer under an excitation at 350 nm for Al^{3+} and Zn^{2+} ions. For Fe^{3+} and Cu^{2+} ions, absorbance values were recorded at 335.0 nm and 382.0 nm, respectively. Job's plots were constructed using fluorescent and absorbance signals to determine the stoichiometry between metal ions and PS. To elucidate the binding mechanism, the solutions of the complex were dried under vacuum using a lyophilizer and the dried samples were subject to X-ray photoelectron spectrometer (Kratos Axis Ultra X-ray Photoelectron Spectroscopy (XPS) system).

2.7. Theoretical calculations

The ground-state geometries of the proposed structures between PS to each metal complexes were fully optimized using the density functional theory (DFT) calculation based on the long-range corrected exchange–correlation function at B3LYP (Kohn et al., 1965) with mixed basis sets. In these mixed basis sets, the effective core potential (ECP) LANL2DZ was set for Al^{3+} and Fe^{3+} ions (Pritchard et al., 2019), and the 6–311++G(d,p) was set for the

remaining atoms (H, C, O), namely, LANL2DZ/6–311++G(d,p) basis set. The simulated absorption spectra based on their ground state (S_0) geometries were calculated using time-dependent B3LYP or TD-B3LYP at the same basis as for the experimental spectrum. Then, to calculate the emission spectra, the geometry optimization was performed for the first excited-state (S_1) using the TD-B3LYP at the same basis set. The solvent effects were evaluated using a non-equilibrium implementation of the conductor-like polarizable continuum model (C-PCM) from the self-consistent reaction field (SCRF) procedure in water solution (Cossi et al., 2003). All aforementioned computations were performed using the Gaussian 09 program package (Frisch et al., 2009).

3. Results and discussion

3.1. Pinostrobin extraction and characterization

PS is a major compound found in rhizomes of fingerroots. The extracts eluted from different liquid chromatographic fractions were investigated and comparatively estimated the amount of PS using thin-layer liquid chromatography (TLC) with standard PS. It was found that the second fraction contained the highest concentration of PS, and was further purified by recrystallization. The white powder of the purified PS was obtained with a yield of 0.52 %. Analytical techniques including NMR, FTIR, and MS were performed to confirm the structure of the compound.

Both ^{1}H NMR (500 MHz, DMSO d_6) and ^{13}C NMR (125 MHz, DMSO d_6) were performed to characterize the structure of the purified compound. The ^{1}H NMR spectrum revealed the presence of a hydroxyl proton signal at δ 12.10 (1H, s) and aromatic proton signals at δ 7.53 (2H, brd, J = 7.2 Hz, H-2′, H-6′), δ 7.44 (2H, brt, J = 7.4 Hz, H-3′, H-5′) and δ 7.40 (1H, brt, J = 7.2 Hz, H-4′) ppm assignable to monosubstituted benzene. The aromatic proton signals at δ 6.16 (1H, brd, J = 2.0 Hz, H-8) and δ 6.11 (1H, brd, J = 2.1 Hz, H-6) ppm were assignable to aromatic protons of ring A (Fig. 1). The oxymethine proton resonated at δ 5.64 (1H, brd, J = 12.7 Hz, H-2) ppm, and methylene proton signal appeared at δ 3.29–3.35 (1H, dd, J = 17.1, 4.4 Hz, H-3b) and δ 2.85–2.81 (1H, dd, J = 17.1, 3.0 Hz, H-3a) ppm (Fig.S1(a-b), ESI). Additionally, ^{1}H NMR spectrum showed one methoxyl group at δ 3.80 (3H, s). These signals corresponded to the structure of PS shown in Fig. 1. Signals of chemical shift from ^{13}C NMR are as follows: δ 42.1 (C-3), 55.9 (OCH$_3$), 78.5 (C-2), 93.8 (C-8), 94.7 (C-6), 102.6 (C-4a), 126.6 (C-2′, C-6′), 128.5 (C-3′, C-5′), 128.6 (C-4′), 138.5 (C-1′), 162.6 (C-8a), 163.2 (C-5), 167.4 (C-7), 196.5 (C-4).

The IR spectrum displayed absorption bands of carbonyl (C = O), C = C aromatic, and ether (C-O-C) at 1642, 1619 (Mohammed et al., 2018) and 1157 cm^{-1}, respectively. The high resolution electrospray mass spectrum showed [M + Na]$^+$ at m/z 293.0791, corresponding to the molecular formula of pinostrobin, C$_{16}$H$_{14}$NaO$_4$ (Fig.S1(c-d), ESI).

Optical properties in relation to absorption and fluorescence spectra of PS were recorded. PS exhibited two characteristic maximum absorption (λ_{max}) of flavonoid at 285.0 nm relating to $\pi \to \pi$ * transition localized within ring A and ring C, and at 335.0 nm corresponding to n $\to \pi$ * transition of carbonyl group in ring C (Jomová et al., 2019). However, the fluorescence of PS in 50 % ethanol:H$_2$O was rather weak (Fig. 2).

3.2. Optical behaviors of pinostrobin in the presence of metal ions

With electron-donating property of oxygen of the hydroxyl and carbonyl groups, PS has potential to form a complex with metal ions (Jomová et al., 2019; Kasprzak et al., 2015). To monitor the interaction between PS and different metal ions, optical changes of PS in the presence of metal ions were investigated. Among the studied metal ions, Fe^{3+} ion and Cu^{2+} ions caused a color change of PS from colorless to dark brown and light green, respectively, as shown in Fig. 3. In the case of Cr^{6+}, Fe^{2+}, and Co^{2+} ions, the colors of the mixture solutions appeared as the colors of metal ions themselves.

Fluorescence emission of the metal ion-added PS solutions was recorded. Fluorescence spectra of the mixtures other than Al^{3+} and Zn^{2+}were not significantly different from that of the PS blank solution. Al^{3+} and Zn^{2+} ions caused an emission enhancement of the PS solution with the maximum emission of 485.0 nm and 538.0 nm, respectively (Fig. 4). Therefore, optical properties of the PS solution with Al^{3+} and Zn^{2+} ions (based on fluorescence emission) and Fe^{3+} and Cu^{2+} (based on UV–Vis absorption) were further investigated.

3.3. Optimum conditions for the application of pinostrobin as an optical probe for metal ion detection

3.3.1. Effects of pH on metal ion detection

Complex formation is generally pH-dependent. Thus, the effect of different pH values on absorption spectra of Cu^{2+} and Fe^{3+} complexes, and fluorescence spectra of Al^{3+} and Zn^{2+} complexes was monitored. There were no significant changes in optical spectra in the free PS ligand mixed with a blank solution of pH 3 to 9 in the ratio of 1:1 (Fig. S2, ESI). In the presence of Cu^{2+} and Fe^{3+} ions, the absorption spectra of the complexes were different from that of the free ligand (Fig. 5). However, the Fe^{3+} complex showed the same absorption spectrum throughout the pH range from 3 to 9 (Fig.S3, ESI), but the spectra of Cu^{2+} complex changed when pH increased. At pH between 7 and 9, the signal at 335.0 nm decreased and that at 382.0 nm increased compared to the lower pH range (Fig. S4, ESI).

The optimum pH for Al^{3+} and Zn^{2+} detection was determined via fluorescence spectrometer. The fluorescence intensity of the Al^{3+} complex was considerably enhanced over the pH range from 3 to 9 compared to that of the free ligand. The intensity at pH 3 was slightly less than others. The intensity of the fluorescence spectra of the Zn^{2+} complex increased slightly at pH 3–5, and significantly increased at pH 7–9 compared to that of the free ligand. Therefore, pH 7 was chosen for further study of metal ion determination.

3.3.2. Effects of concentration of pinostrobin on metal ion detection

The influence of PS concentration on metal ion detection was investigated because it resulted in changes in optical properties of the complex and solubility of PS. To optimize the concentration of PS, enhancement of fluorescence emission in terms of relative fluorescence intensity of Al^{3+} complex at the emission wavelength of 538.0 nm was monitored over the PS concentrations from 50 ppm to 1000 ppm (Fig. S5, ESI). The PS concentration of 100 ppm provided the largest percent of emission enhancement.
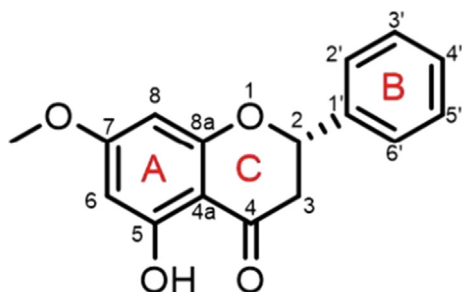
Fig. 1. Structure of pinostrobin.
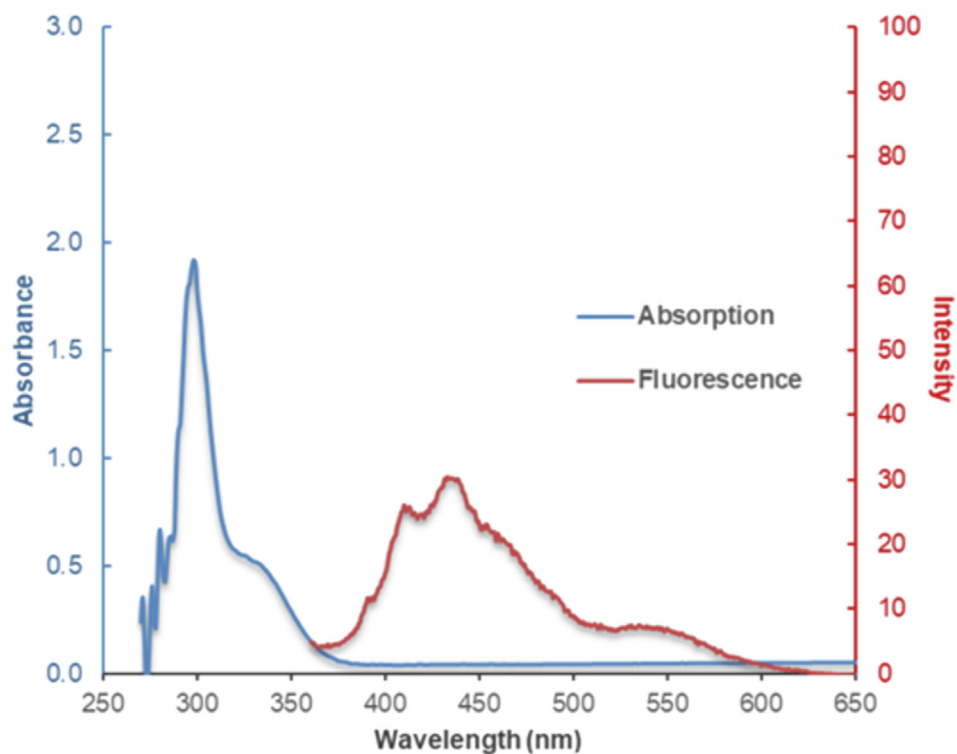
Fig. 2. Absorption and fluorescence spectra of PS solution.

Fig. 3. Appearance of mixture solutions of 100 ppm of PS (ligand) and 100 ppm of different metal ions.

Therefore, 100 ppm of PS concentration was chosen for further studies.

PS is soluble in organic solvent while metal ions are generally highly soluble in water. To facilitate the metal complex formation, the aqueous solution of Al^{3+}, a representative of other metal ions, was mixed with PS solution. High concentration of PS can cause precipitation after mixing with the Al^{3+} aqueous solution. A suitable organic solvent for dissolving PS was also investigated. We found that ethanol was the most suitable solvent for PS because of good solubility with no precipitation of PS at high concentration up to 1000 ppm after adding the Al^{3+} aqueous solution. Moreover, it is a more environmental friendly organic solvent.

3.3.3. Effects of reaction time

The complex formation time to reach equilibrium was investigated to obtain an optimal reaction time between metal ions and PS. The reaction kinetic of the complexes of Fe^{3+} and Al^{3+} through absorbance and fluorescence emission, respectively, was recorded. The maximum absorbance of Fe^{3+} complex at 335.0 nm was achieved within 15 min (Fig. S6, ESI). For the Al^{3+} complex, the flu-

orescence intensity gradually increased and became steady after 24 min of reagents mixing. Thus, the reaction times to obtain the maximum signals for Fe^{3+} and Al^{3+} were at least 15 min and 24 min, respectively, prior to spectroscopic measurements.

3.4. Application of pinostrobin for metal ion measurement in environmental samples

The calibration curves of Cu^{2+}, Fe^{3+}, Al^{3+}, and Zn^{2+} ions were constructed by measuring either absorbance or fluorescence emission of the complexes. Poor detection sensitivity of standard Cu^{2+} and Zn^{2+} solutions was obtained (data not shown). Hence, only Fe^{3+} and Al^{3+} were determined in environmental water samples (tap water, groundwater, and canal water) through the PS complex formation. We found that the absorbance of Fe^{3+}- $(PS)_n$ at 335.0 nm was linearly proportional to the concentration of Fe^{3+} ions (Fig. 6a), while fluorescence intensity of Al^{3+}- $(PS)_n$ at 538.0 nm increased exponentially with increasing concentration of Al^{3+} ions (Fig. 6b). Therefore, the linear correlation between the fluorescence intensities and concentrations of Al^{3+} in terms of logarithmic function was
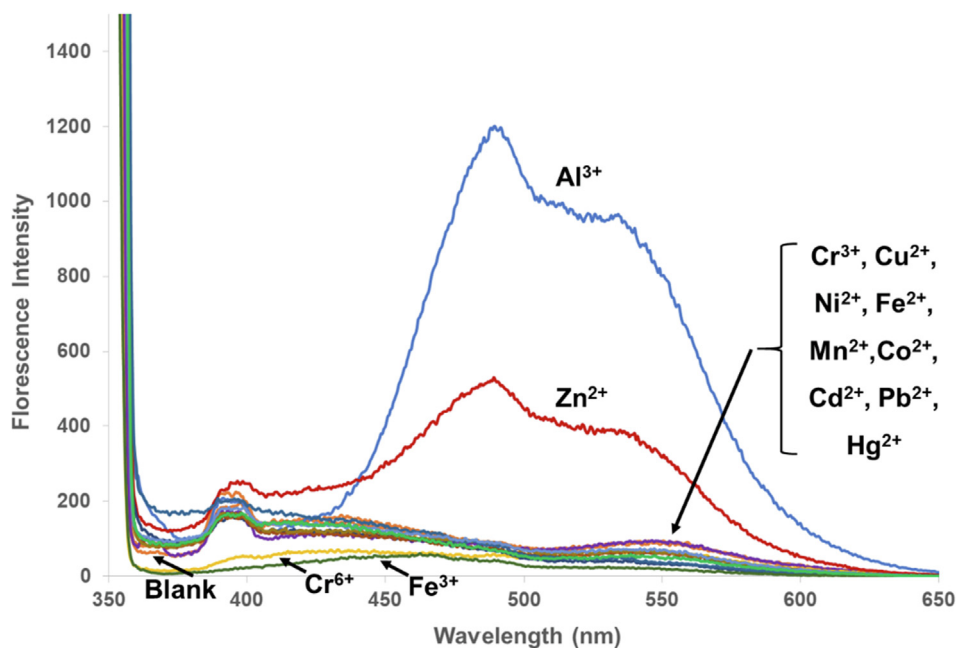
Fig. 4. Fluorescence spectra of mixture solutions of 100 ppm of pinostrobin and 100 ppm of different metal ions.
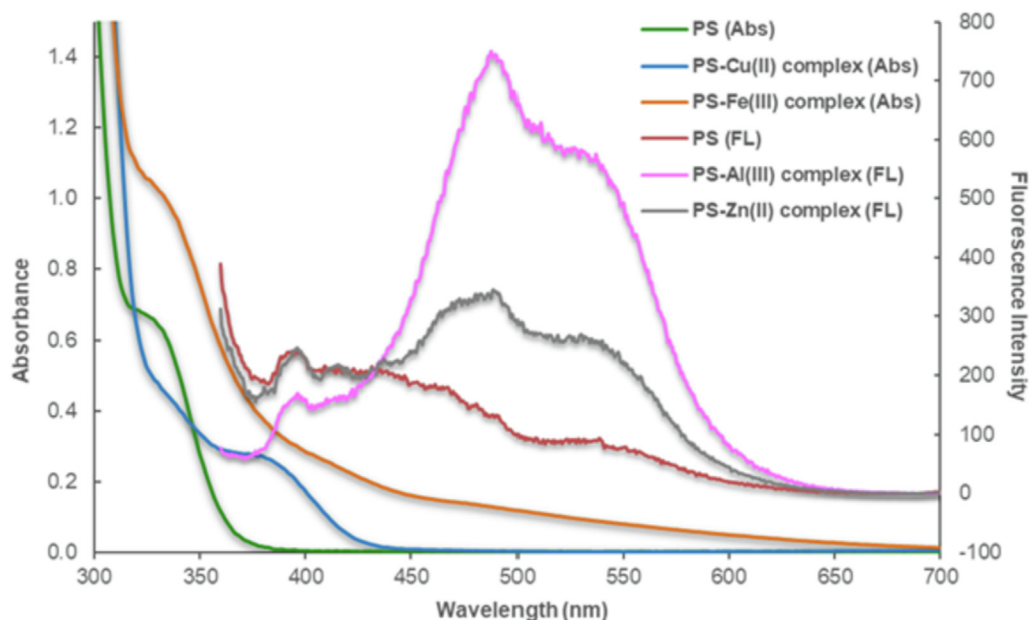
Fig. 5. Absorption (Abs) spectra of free ligand (PS) and Cu^{2+} and Fe^{3+} complexes; and fluorescence (FL) spectra of free ligand (PS) and Al^{3+} and Zn^{2+} complexes.

obtained. Linearity ranges of Fe^{3+} and Al^{3+} detection were 1–150 ppm and 0.05–100 ppm, respectively. Limit of detection (LOD) and limit of quantification (LOQ) for Fe^{3+} were 0.27 ppm and 0.90 ppm, respectively, while those for Al^{3+} were 0.02 ppm and 0.05 ppm, respectively. The LOD and LOQ were calculated based on the standard deviation (SD) at the lowest concentrations of linearity ranges of these ions and the slope of their calibration curves.

The metal ions contaminated in samples of natural water including tap water, groundwater, and canal water were evaluated.

A series of samples with different concentrations of metal ions were determined using the proposed method in comparison to the results obtained from ICP-OES. As shown in Table 1, Fe^{3+} ions were found in the range of 0.30–0.37 ppm, while Al^{3+} ions were not detected in the selected natural water determined by ICP-OES. Using the developed method, Fe^{3+} ions were detected at a significantly lower amount than by ICP-OES. The differences in detection may be due to the fact that the water samples contained less amount of Fe^{3+} ions than the LOQ of the developed method, leading to errors in the determination. In addition, the much higher
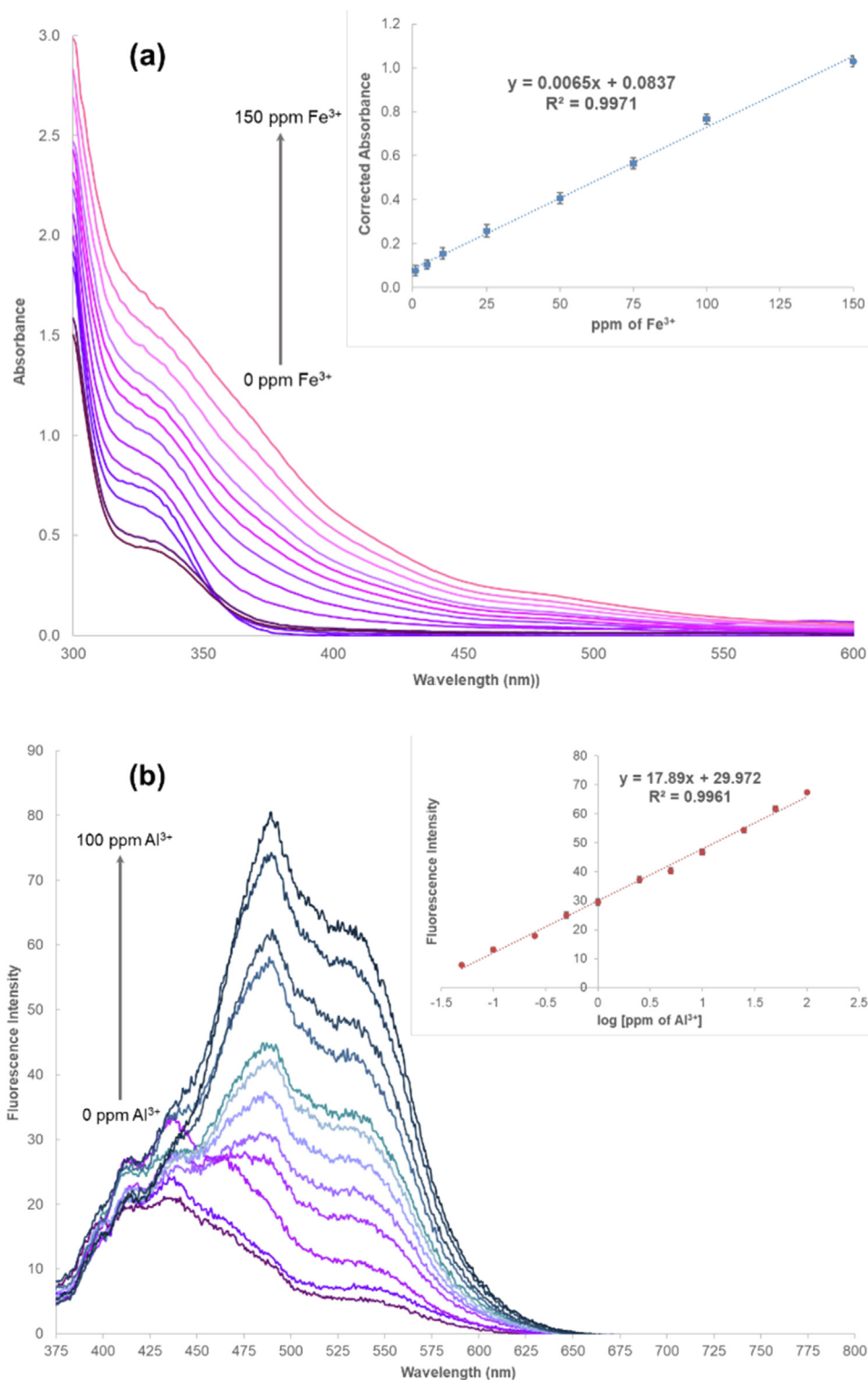
Fig. 6. (a) Absorption spectra of Fe^{3+}-$(PS)_n$ obtained from different concentrations of Fe^{3+} ions, and (b) fluorescence spectra of Al^{3+}-$(PS)_n$ obtained from different concentrations of Al^{3+} ions with their calibration curves (inset).

detection value by ICP-OES was also attributed to ICP-OES not being able to differentiate between Fe^{3+} and Fe^{2+}, resulting in an overestimation compared to the more selective developed method. The recoveries of Fe^{3+} and Al^{3+} ions in the real samples were between 91.00 and 107.08 % and 92.00–108.00 %, respectively. At concentrations of metal ions higher than the LODs, there were no significant differences in metal ion amounts determined by the two methods, indicating that the developed method was practical

and applicable for the detection of Fe^{3+} and Al^{3+} in natural water samples.

3.5. Binding mechanism between pinostrobin and metal ions

To understand the reaction between PS and metal ions, the complex formation mechanism was studied using several analytical techniques including FTIR, X-ray photoelectron spectrometry

Table 1
Amounts of Fe^{3+} and Al^{3+} in real water samples determined by ICP-OES and the proposed method.

Sample	Added metal standard (ppm)	Fe^{3+} determination			Al^{3+} determination		
		ICP-OES (ppm)	Proposed method (ppm)	Recovery (%)	ICP-OES (ppm)	Proposed method (ppm)	Recovery (%)
Tap water	0.0	0.34 ± 0.01	0.15 ± 0.06	–	0.00	0.00	–
	1.0	1.26 ± 0.02	1.17 ± 0.12	102.0	0.94 ± 0.02	0.92 ± 0.08	92.00
	25.0	26.83 ± 0.61	24.76 ± 1.05	98.44	24.77 ± 0.57	23.84 ± 0.98	95.36
Groundwater	0.0	0.37 ± 0.02	0.27 ± 0.05	–	0.00	0.00	–
	1.0	1.32 ± 0.01	1.21 ± 0.16	94.00	0.98 ± 0.02	0.94 ± 0.10	94.00
	25.0	26.68 ± 0.12	27.04 ± 1.13	107.08	23.97 ± 0.18	24.63 ± 1.22	98.52
Canal water	0.0	0.30 ± 0.00	0.18 ± 0.05	–	0.00	0.00	–
	1.0	1.22 ± 0.02	1.09 ± 0.19	91.00	0.93 ± 0.01	1.08 ± 0.23	108.00
	25.0	26.02 ± 0.32	24.84 ± 1.21	98.64	25.20 ± 0.54	24.21 ± 1.30	96.84
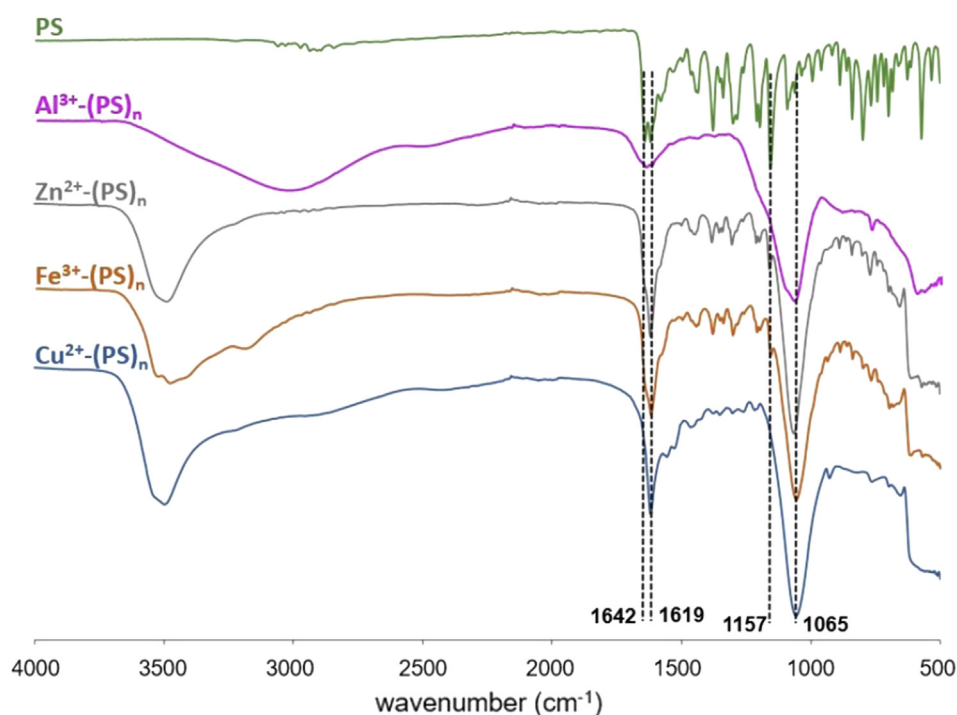
Fig. 7. ATR-FTIR spectra of PS powder in comparison to PS complex with different metal ions (M^{n+}- $(PS)_n$).

(XPS), UV–Vis spectrophotometry, and fluorescence spectrophotometry. The metal complexes were characterized using FTIR, and the spectra showed significant changes compared to that of blank PS (Fig. 7). The peak of C = O stretching at 1642 cm^{-1} disappeared, and a strong peak of 1065 cm^{-1} developed, which corresponds to deformational vibration of C-OH. These changes indicated an interaction between PS and metal ions through functional groups C = O and C-OH. The signals at 1619 cm^{-1} and 1157 cm^{-1} assigned to C = C and C-O-C, respectively, remained at the same wavenumber, which confirms non-complex formation sites. Moreover, the O–H stretching band of the complexes appeared at 3000–3500 cm^{-1}, indicating the presence of water crystallization in the complexes (Mathiyalagan et al., 2021).

An XPS analysis was conducted on PS before and after the metal complex formation to elucidate the interaction mechanism. The photoelectron spectra of C 1 s (Fig. S7, ESI) and O 1 s (Fig. 8) were recorded. In free PS powder, the major peaks appeared at binding energies B.E.) of 531.750 eV and 533.233 eV, corresponding to –OH of the phenol hydroxyl group and C-O-C in the aromatic ring, respectively. A minor peak at 534.484 eV was detected, indicating an adsorbed water content 534.484 eV was detected, indicating an adsorbed water content in the sample. The same trend of B.E. of O

1 s was observed in all PS complexes with different metal ions [Table 2]. The B.E. of O 1 s of phenol hydroxyl group significantly increased (ΔB.E. > 0.5), which indicates the coordinating formation to metal ions, while those of the ester group remained the same (ΔB.E. < 0.5). Therefore, the ester group was not involved in the complex formation. In the case of the Zn complex, the lower B.E. of O 1 s at 530.429 eV suggested the presence of a hydroxide species of Zn. This hydroxide species was less soluble compared to other metal hydroxide forms of other metal ions at pH $\sim$ 7 (Marchioretto et al., 2005). In addition, some of hydroxyl groups from the phenol moiety remained unbound to Zn ions as evident by the peak at 531.466 eV, which is close to that of free ligand. The results obtained from the XPS analysis showed good agreement with those from FTIR, suggesting that the hydroxyl and carbonyl groups of PS are the binding sites for complex formation with metal ions, causing the changes in optical property of PS.

The stoichiometry of metal ions and PS was determined using the continuous variation method (Job's plot). A correlation between relative absorbance and mole fraction of metal ion was plotted for Fe^{3+} and Cu^{2+} complexes, while the values of relative fluorescence intensity were used for Al^{3+} and Zn^{2+} complexes. All complexes were formed with the ratio of metal to PS of 1:2
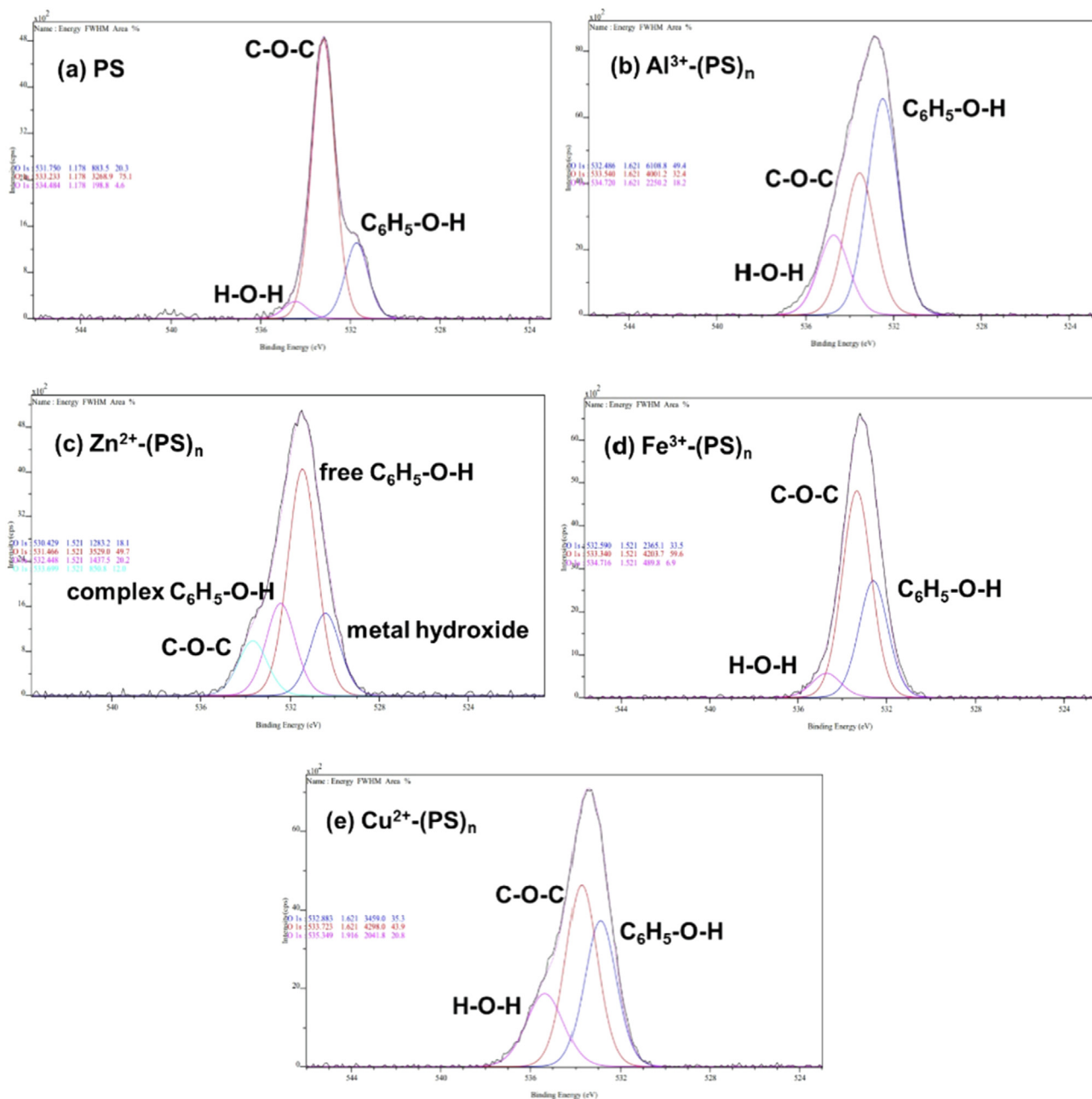
Fig. 8. Deconvoluted peaks of O 1 s of PS (a), and PS complexes with metal ions (b-e).

Table 2
Assignments of main spectral bands based on their binding energies (B.E.) of oxygen and carbon atoms of PS before and after the metal ion complex formation.

B.E. (eV)	O 1 s			
Assignment	Metal hydroxide (Dupin et al., 2000; Gomez-Bolivar et al., 2019)	C_6H_5-O'H (Shen et al., 2013)	C-O'-C (Far et al., 2017)	H-O-H (adsorbed) (Shen et al., 2013)
PS (free)		531.750	533.233	534.484
Al^{3+}- $(PS)_n$	–	532.486	533.540	534.720
Zn^{2+}- $(PS)_n$	530.429	531.466/532.448	533.699	–
Fe^{3+}- $(PS)_n$	–	532.590	533.340	534.716
Cu^{2+}- $(PS)_n$	–	532.883	533.723	535.349

(Fig. S8, ESI). The structure of the complex is proposed in Fig. 9. Oxygen atoms of the carbonyl and hydroxyl groups from two molecules of PS bind to the center metal ion in a planar geometry.

In addition, molecules of water, as detected in the complex crystal, attach to the center metal ion causing the formation of octahedral complex. Complex formation between Fe^{3+} or Cu^{2+} with PS caused
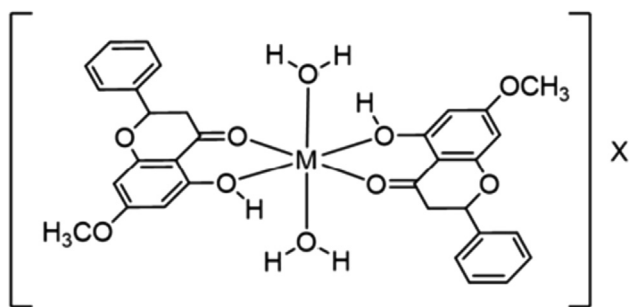
Fig. 9. A Proposed structure of complex formation between metal ion and PS; M = metal ions including Fe^{3+}, Cu^{2+}, Al^{3+}, Zn^{2+}, and X = counter anion.

the change in color of PS from colorless to brown and green, respectively. The shift in color can be explained using the crystal field and charge transfer theory. Coordination with PS results in *d*-orbital splitting of Fe^{3+} ion, leading to *d-d* transition and thus enhancing the absorbance at 500–600 nm. In addition, an increase in absorbance at 300 – 400 nm results from the charge transfer of PS (ligand) to d orbital of Fe^{3+}. For the Cu^{2+} complex, a new peak appears at 375 nm, corresponding to the green color because of the *d-d* transition of Cu^{2+} ion. In the case of Al^{3+} and Zn^{2+} complexes, the solution remained colorless because there is no electron filled in d orbitals of Al^{3+} ion, while fully filled in d orbitals of Zn^{2+} ion. As a result, no *d-d* transition occurs.

Originally, a solution of PS exhibits a weak fluorescence emission. Complexing with Al^{3+} and Zn^{2+} led to a significantly enhancement of fluorescence. This is possibly attributed to the inhibition of photo-induced ultrafast proton transfer or tautomerization process (Park et al., 2016) between the hydroxyl group and carbonyl group

within the molecule of PS. In addition, the specificity of PS to Al^{3+} and Zn^{2+} caused a significant increase in fluorescence intensity due to the enhanced mobility of electrons in the structure of the complex and the internal electronic transition was reduced (Jianbo et al., 2018; Ravi Kishore et al., 2002).

3.6. Theoretical study of complex structure

To confirm the structure of the proposed complex, simulated absorption spectra based on ground state (S_0) geometries of free PS and its complexes with Fe^{3+} and Al^{3+} ions were calculated using time-dependent B3LYP or TD-B3LYP at the same basis set as the experimental spectra (Fig. S9, ESI). The results showed that the calculated absorption spectrum of Fe^{3+} complex matched that of the experimental spectrum, while acceptable differences of approximately 30 nm of maximum absorption was observed between the experimental spectrum and calculated spectrum of the Al^{3+} complex. Thus, the proposed complex structure is likely accurate. The energy gap (ΔE_{gap}) between the highest occupied molecular orbital (HOMO) and the lowest unoccupied molecular orbital (LUMO) is an indication of the stability of a molecule and its resistivity to light radiation. The predicted ΔE_{gap} values and the spatial distributions of the Fe^{3+} (Fig. 10) and Al^{3+} complexes at ground states and the first singlet excited state of Al^{3+} complex (Fig. S10, ESI) in an aqueous solution were calculated. The results indicated that the formation between PS and Fe^{3+} was the most stable coordination complex at ground state as the smallest ΔE_{gap} was obtained, and the energy significantly decreased compared to that of a free PS molecule. This observation aligns with the experimental results, which indicates that the binding of Fe^{3+} to PS stabilizes the system due to a decrease in the HOMO-LUMO energy gap of the complex. As shown in Fig. 10, the π electrons at HOMO are mainly distributed on PS rings whereas those at the LUMO are mainly dis-

HOMO-LUMO of free PS $(\Delta E_{gap} = 0.174$ eV$)$

HOMO-LUMO of $(PS_2\text{-}Fe^{3+})\cdot 2H_2O$ $(\Delta E_{gap} = 0.063$ eV$)$
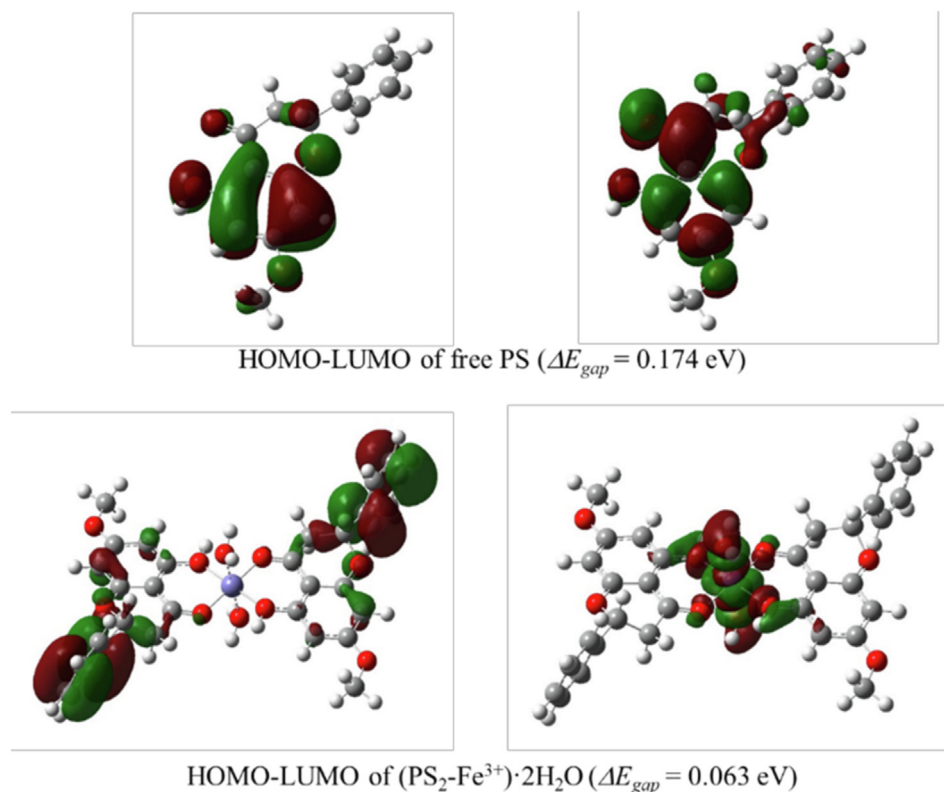
Fig. 10. The HOMO and LUMO orbitals at ground state and the energy gaps (ΔE_{gap}) of free PS and Fe^{3+} complexes calculated using the TD-B3LYP/LANL2DZ/6–311++G(d,p) method in CPCM water model.

tributed on the metal ions. For the Al^{3+} complex at ground state, the ΔE_{gap} (0.143 eV) was also lower than that of free PS, but considerably higher than that of Fe^{3+}, corresponding to the weak absorption behavior of the Al^{3+} complex. However, the ΔE_{gap} (0.122 eV) of Al^{3+} complex at the first excited state was smaller than that at ground state. This could explain the preferable fluorescence behavior of the Al^{3+} complex. In addition, binding energies of both Fe^{3+} and Al^{3+} complexes were calculated, and the respective values of -11.45 eV and -19.37 eV were obtained, indicating high stability of the structure and geometry of the metal complexes.

4. Conclusions

This work presented a novel approach of using a colorless and non-luminescent PS molecule, a natural flavonoid, as an optical sensor for metal ion determination. The PS turned on its optical behaviour upon complex formation with specific metal ions. The resulting Fe^{3+} and Cu^{2+} complexes caused a color change, while Al^{3+} and Zn^{2+} complexes caused an enhancement of fluorescence intensity. With these unique optical properties, PS can be applied as a low cost and non-toxic probe for metal ion detection with high sensitivity and selectivity. The proposed approach would be useful for Fe^{3+} and Al^{3+} quantification in drinking water and natural water samples to ensure that they are safe for consumption (below 0.3 ppm of Fe^{3+} and 0.1 ppm of Al^{3+} as recommended by World Health Organization (WHO) and the Environmental Protection Agency (EPA) of the United States (Ji et al., 2019)). In addition, this study revealed that the carbonyl and hydroxyl groups of PS play an important role in complex formation with metal ions. The results from the experimental and theoretical studies were congruent, showing the formation of octahedral complexes of a center metal ion binding to two molecules of PS and water.

Declaration of Competing Interest

The authors declare that they have no known competing financial interests or personal relationships that could have appeared to influence the work reported in this paper.

Acknowledgments

Appendix A. Supplementary material

Supplementary data to this article can be found online at https://doi.org/10.1016/j.arabjc.2023.105321.

References

Adusei-Gyamfi, J., Ouddane, B., Rietveld, L., Cornard, J.P., Criquet, J., 2019. Natural organic matter-cations complexation and its impact on water treatment: A critical review. Water Res. 160, 130–147.

Ali, H., Khan, E., 2018. Bioaccumulation of non-essential hazardous heavy metals and metalloids in freshwater fish. Risk to human health. Environ. Chem. Lett. 16, 903–917.

Ali, H., Khan, E., Ilahi, I., 2019. Environmental chemistry and ecotoxicology of hazardous heavy metals: environmental persistence, toxicity, and bioaccumulation. J. Chem. https://doi.org/10.1155/2019/6730305.

Assubaie, F.N., 2015. Assessment of the levels of some heavy metals in water in Alahsa Oasis farms, Saudi Arabia, with analysis by atomic absorption spectrophotometry. Arab. J. Chem. 8, 240–245.

Cossi, M., Rega, N., Scalmani, G., Barone, V., 2003. Energies, structures, and electronic properties of molecules in solution with the C-PCM solvation model. J. Comput. Chem. 24, 669–681. https://doi.org/10.1002/jcc.10189.

Dias, M.C., Pinto, D.C.G.A., Silva, A.M.S., 2021. Plant flavonoids: Chemical characteristics and biological activity. Molecules 26, 5377. https://doi.org/10.3390/molecules26175377.

Dupin, J.C., Gonbeau, D., Vinatier, P., Levasseur, A., 2000. Systematic XPS studies of metal oxides, hydroxides and peroxides. PCCP 2, 1319–1324.

Edelstein, M., Ben-Hur, M., 2018. Heavy metals and metalloids: sources, risks and strategies to reduce their accumulation in horticultural crops. Sci. Hortic. 234, 431–444.

Far, H.M., Donthula, S., Taghvaee, T., Saeed, A.M., Garr, Z., Sotiriou-Leventis, C., Leventis, N., 2017. Air-oxidation of phenolic resin aerogels: backbone reorganization, formation of ring-fused pyrylium cations, and the effect on microporous carbons with enhanced surface areas. RSC Adv. 7, 51104–51120.

Frisch MJ, Trucks GW, Schlegel HB, et al., (2009) Gaussian 09, Revision B.01, Gaussian: Wallingford, CT.

Gomez-Bolivar, J., Mikheenko, I.P., Orozco, R.L., Sharma, S., Banerjee, D., Walker, M., Hand, R.A., Merroun, M.L., Macaskie, L.E., 2019. Synthesis of Pd/Ru bimetallic nanoparticles by Escherichia coli and potential as a catalyst for upgrading 5-hydroxymethyl furfural into liquid fuel precursors. Front. Microbiol. 10, 1276. https://doi.org/10.3389/fmicb.2019.01276.

He, Z., Yin, H., Chang, C.C., Wang, G., Liang, X., 2020. Interfacing DNA with gold nanoparticles for heavy metal detection. Biosensors (basel) 10, 167. https://doi.org/10.3390/bios10110167.

Ihedioha, J.N., Ukoha, P.O., Ekere, N.R., 2017. Ecological and human health risk assessment of heavy metal contamination in soil of a municipal solid waste dump in Uyo, Nigeria. Environ. Geochem. Health 39, 497–515.

Jaishankar, M., Tseten, T., Anbalagan, N., Mathew, B.B., Beeregowda, K.N., 2014. Toxicity, mechanism and health effects of some heavy metals. Interdiscip. Toxicol. 7, 60–72.

Ji, W., Zhu, Z., Dong, S., Nie, J., Du, B., 2019. Optical detection of Fe3+ ions in aqueous solution with high selectivity and sensitivity by using sulfasalazine functionalized microgels. Sensors (basel) 19, 4223. https://doi.org/10.3390/s19194223.

Jianbo, H., Tingting, Z., Yongjing, C., Yuanyuan, Z., Weiqing, Y., Menglin, M., 2018. Study on relationship between fluorescence properties and structure of substituted 8-hydroxyquinoline zinc complexes. J. Fluoresc. 28, 1121–1126.

Jing, Z., Qi, R., Liu, C., Ren, P., 2017. Study of interactions between metal ions and protein model compounds by energy decomposition analyses and the AMOEBA force field. J. Chem. Phys. 147, 161733. https://doi.org/10.1063/1.4985921.

Jomová, K., Hudecova, L., Lauro, P., Simunkova, M., Alwasel, S.H., Alhazza, I.M., Valko, M., 2019. A switch between antioxidant and prooxidant properties of the phenolic compounds myricetin, morin, 3′,4′-dihydroxyflavone, taxifolin and 4-hydroxy-coumarin in the presence of copper(II) ions: A spectroscopic, absorption titration and DNA damage study. Molecules 24, 4335. https://doi.org/10.3390/molecules24234335.

Kanchanapiboon, J., Kongsa, U., Pattamadilok, D., Kamponchaidet, S., Wachisunthon, D., Poonsatha, S., Tuntoaw, S., 2020. Boesenbergia rotunda extract inhibits Candida albicans biofilm formation by pinostrobin and pinocembrin. J. Ethnopharmacol. 261, 113193. https://doi.org/10.1016/j.jep.2020.113193.

Kasprzak, M.M., Erxleben, A., Ochocki, J., 2015. Properties and applications of flavonoid metal complexes. RSC Adv. 5, 45853–45877.

Kejík, Z., Kaplánek, R., Masařík, M., Babula, P., Matkowski, A., Filipenský, P., Veselá, K., Gburek, J., Sýkora, D., Martásek, P., Jakubek, M., 2021. Iron Complexes of flavonoids-antioxidant sapacity and beyond. Int. J. Mol. Sci. 22, 646. https://doi.org/10.3390/ijms22020646.

Khater, M., Ravishankar, D., Greco, F., Osborn, H.M., 2019. Metal complexes of flavonoids: their synthesis, characterization and enhanced antioxidant and anticancer activities. Future Med. Chem. 11, 2845–2867.

Kohn, W., Sham, L.J., 1965. Self-consistent equations including exchange and correlation effects. Phys. Rev. 140, A1133. https://doi.org/10.1103/PhysRev.140.A1133.

Kumar, S., Pandey, A.K., 2013. Chemistry and biological activities of flavonoids: an overview. Sci. World J. https://doi.org/10.1155/2013/162750.

Li, C., Ulrich, M., Liu, X., Wurst, K., Müller, T., Kräutler, B., 2014. Blue transition metal complexes of a natural bilin-type chlorophyll catabolite. Chem. Sci. 5, 3388–3395.

Liang, J., Wang, Q., Huang, B., 2004. Concentrations of hazardous heavy metals in environmental samples collected in Xiamen, China, as determined by vapor generation non-dispersive atomic fluorescence spectrometry. Anal. Sci. 20, 85–88.

Liu, J., Zhang, Q., Xue, W., Zhang, H., Bai, Y., Wu, L., Zhai, Z., Jin, G., 2019. Fluorescence characteristics of aqueous synthesized tin oxide quantum dots for the detection of heavy metal ions in contaminated water. Nanomaterials (basel) 9, 1294. https://doi.org/10.3390/nano9091294.

Marchioretto, M.M., Bruning, H., Rulkens, W., 2005. Heavy metals precipitation in sewage sludge. Sep. Sci. Technol. 40, 3393–3405.

Massadeh, A.M., El-Rjoob, A.W.O., Gharaibeh, S.A., 2020. Analysis of selected heavy metals in tap water by inductively coupled plasma-optical emission spectrometry after pre-concentration using Chelex-100 ion exchange resin. Water Air Soil Pollut. 231, 243. https://doi.org/10.1007/s11270-020-04555-5.

Mathiyalagan, S., Mandal, B.K., 2021. Stability comparison of quercetin and its metal complexes and their biological activity. Biointerface Res. Appl. Chem. 11, 7890–7902.

Mohammed, I.A., Abdullah, H., Akhtar, M., Hamid, H., 2018. Characterization of two chalcone derivatives isolated from finger root with nutraceutical potentials. Int. J. Adv. Res. 6, 1089–1094.

Odika, P.O., Anike, O.L., Onwuemesi, A.G., Odika, N.F., Ejeckam, R.B., 2020. Assessment of environmental geochemistry of lead-zinc mining at Ishiagu area, Lower Benue Trough, southeastern Nigeria. Earth Sci. Res. 9, 31–44.

Park, S.Y., Ghosh, P., Park, S.O., Lee, Y.M., Kwak, S.K., Kwon, O.H., 2016. Origin of ultraweak fluorescence of 8-hydroxyquinoline in water: photoinduced ultrafast proton transfer. RSC Adv. 6, 9812–9821.

Petukh, M., Alexov, E., 2014. Ion binding to biological macromolecules. Asian J. Phys. 23, 735–744.

Pritchard, B.P., Altarawy, D., Didier, B., Gibson, T.D., Windus, T.L., 2019. New basis set exchange: an open, up-to-date resource for the molecular sciences community. J. Chem. Inf. Model. 59, 4814–4820. https://doi.org/10.1021/acs.jcim.9b00725.

Qayoom, A., Kazmi, S.A., Ali, S.N., 2017. Turmeric powder as a natural heavy metal chelating agent: surface characterisation. Pak. J. Sci. Ind. Res. A: Phys. Sci. 60, 1–8.

Ravi Kishore, V.V.N., Aziz, A., Narasimhan, K.L., Periasamy, N., Meenakshi, P.S., Wategaonkar, S., 2002. On the assignment of the absorption bands in the optical spectrum of Alq3. Synth. Met. 126, 199–205.

Rodríguez-Arce, E., Saldías, M., 2021. Antioxidant properties of flavonoid metal complexes and their potential inclusion in the development of novel strategies for the treatment against neurodegenerative diseases. Biomed. Pharmacother. 143, 112236. https://doi.org/10.1016/j.biopha.2021.112236.

Rosdianto, A.M., Puspitasari, I.M., Lesmana, R., Levita, J., 2020. Bioactive compounds of Boesenbergia sp. and their anti-inflammatory mechanism: A review. J. Appl. Pharm. Sci. 10, 116–126.

Shen, L., Chen, M., Hu, L., Chen, X., Wang, J., 2013. Growth and stabilization of silver nanoparticles on carbon dots and sensing application. Langmuir 29, 16135–111640.

Shi, Y., Jiang, W., Auckloo, B.N., Wu, B., 2015. Several classes of natural products with metal ion chelating ability. Curr. Org. Chem. 19, 1935–1953.

Siangproh, W., Chailapakul, O., Songsrirote, K., 2016. Simple and fast colorimetric detection of inorganic arsenic selectively adsorbed onto ferrihydrite-coated silica gel using silver nanoplates. Talanta 153, 197–202.

Sigurdson, G.T., Robbins, R.J., Collins, T.M., Giusti, M.M., 2016. Evaluating the role of metal ions in the bathochromic and hyperchromic responses of cyanidin derivatives in acidic and alkaline pH. Food Chem. 208, 26–34.

Sigurdson, G.T., Robbins, R.J., Collins, T.M., Giusti, M.M., 2017. Spectral and colorimetric characteristics of metal chelates of acylated cyanidin derivatives. Food Chem. 221, 1088–1095.

Thepmanee, O., Prapainop, K., Noppha, O., Rattanawimanwong, N., Siangproh, W., Chailapakul, O., Songsrirote, K., 2020. A simple paper-based approach for arsenic determination in water using hydride generation coupled with mercaptosuccinic-acid capped CdTe quantum dots. Anal. Methods 12, 2718–2726.

Tüzen, M., 2003. Determination of heavy metals in fish samples of the middle Black Sea (Turkey) by graphite furnace atomic absorption spectrometry. Food Chem. 80, 119–123.

Wang, F., Wang, Z., Kou, C., Ma, Z., Zhao, D., 2016. Responses of wheat yield, macro- and micro-nutrients, and heavy metals in soil and wheat following the application of manure compost on the North China plain. PLoS One. https://doi.org/10.1371/journal.pone.0146453.

Winiarska-Mieczan, A., 2018. Protective effect of tea against lead and cadmium-induced oxidative stress-a review. Biometals 31, 909–926.

Zhang, N., Qiao, R., Su, J., Yan, J., Xie, Z., Qiao, Y., Wang, X., Zhong, J., 2017. Recent advances of electrospun nanofibrous membranes in the development of chemosensors for heavy metal detection. Small 13, 1604293. https://doi.org/10.1002/smll.201604293.